# Fast traveling waves in the phase-field theory: effective mobility approach versus kinetic energy approach

## A Salhoumi[1] and P K Galenko[2,3,4]

[1] University of Hassan II Casablanca, Faculty of Sciences Ben M'Sik, Laboratory of Condensed Matter Physics (LPMC), BP 7955, Casablanca, Morocco
[2] Friedrich-Schiller-Universität Jena, Physikalisch-Astronomische Fakultät, D-07743 Jena, Germany
[3] Ural Federal University, Theoretical and Mathematical Physics Department, Laboratory of Multi-Scale Mathematical Modeling, 620000 Ekaterinburg, Russia

E-mail: ahmedsalhoumi@gmail.com and peter.galenko@uni-jena.de

## Abstract

A phase-field model for small and large driving forces on solidification and melting of a pure substance or alloys is formulated. Derivations of the phase-field model are based on the effective mobility approach and on the kinetic energy approach to analyze fast phase transformation from metastable liquid to solid phase. A hodograph equation (an acceleration-velocity dependent equation of the Gibbs–Thomson type) which predicts the non-linear behavior in the velocity of the crystal–liquid interface is found at the large driving force on transformation and analyzed for different thermodynamic potentials. Traveling wave solutions of this equation are found for double-well and double-obstacle potentials. The velocity-dependent traveling waves as a function of driving force on transformation exhibit non-linearity of the solutions. Namely, in the relationship 'velocity–driving force' exists a maximum at a fixed undercooling which is very well known in the solidification of glass-forming metals and alloys. The predicted solidification velocity is quantitatively compared with the molecular dynamics simulation data obtained by Tang and Harrowell (2013 *Nat. Mater.* **12** 507–11) for the solidification of congruently melting Cu–Zr binary alloy. The comparison confirms a crucial role of local non-equilibrium such as relaxation of gradient flow in the quantitative description of fast phase transformations.

Keywords: traveling wave, phase-field, metastable liquid, interface

(Some figures may appear in colour only in the online journal)

## 1. Introduction

The phenomenon of traveling waves is widely known in phase transformations existing in liquids and solids or chemical reactions and biological systems [1–4]. One of the well-established examples is represented by crystalline fronts invading liquid phases [5], in which, as a particular case, the emission of long-wavelength traveling waves has been detected in directional solidification of a ternary eutectic alloy [6]. In this respect, a big number of investigations were devoted to the theoretical study of traveling waves [7–10], particularly, related to equations of the phase-field theory [11–13].

The first traveling wave solutions in phase-field theory were obtained by Kobayashi [14], Wheeler *et al* [15] and Danilov [16] based on analytical solutions of Montroll [17] and Harrowell and Oxtoby [18]. Further advancements of these solutions in the form of the hyperbolic tangent function and sinus-function were made for various field potentials [19] and for fast phase fields [20, 21].

[4] Author to whom any correspondence should be addressed.

In the present work, we advance the concept of traveling waves further for the fast crystalline fronts invading metastable liquid under the high driving force of phase transformation [5]. The motion of such traveling waves can be so fast that the local bulks of the system under transformation do not reach thermodynamical and/or mechanical equilibrium with the ergodicity breaking [22]. In such a case, a set of independent slow thermodynamic variables (chemical potential, inner energy, phase-field) is extended by the space of independent fast variables which are represented by the kinetic functions such as fluxes and gradient flows [23, 24]. This extension leads to the hyperbolic or parabolic equations having non-local terms in time and in space which represent relaxation to equilibrium in local bulks (temporal relaxation) and/or spatial correlation among these local bulks (spatial non-locality).

To describe the fast crystalline waves propagating into a metastable liquid, we consider a class of hyperbolic equations of the phase-field theory which describes the time delay due to relaxation to thermodynamic equilibrium within the local bulks. This occurs due to the introducing of the gradient flow as a fast thermodynamic variable the relaxation of which describes local temporal relaxation to the thermodynamic equilibrium. The resulting phase-field equation is found from the kinetic energy and extended mobility approaches [25–27] summarized in the present work using double-well and double-obstacle potentials which thermodynamically divide liquid and solid states by the energetic barrier between these states. After an averaging procedure, the hyperbolic phase-field equation is reduced to the hodograph equation which is considered as a generalized Gibbs–Thomson equation realizing a connection of the interface acceleration and velocity with the interface curvature and driving force [28].

The main goal of the present work is to directly compare the hodograph equations derived from the kinetic energy and extended effective mobility approaches which include different thermodynamic potentials energetically dividing liquid and solid phases. After the comparison, the prediction of the hodograph equation relatively the data of atomistic computer simulation will be analyzed. The atomistic data were obtained by Tang and Harrowell [29] using the method of molecular dynamics applied to the problem of fast crystalline interfaces. As a quantitative result, the solution of the hodograph equation will be tested against the atomistic data of modeling for the interface moving with the constant velocity into undercooled congruently melting alloy.

## 2. Basic definitions

Consider an isothermal solidification of a binary alloy consisting of A-atoms (solvent) together with B-atoms (solute) under constant temperature $T$ and constant pressure in a closed system. The overall solute concentration $C$ is described by

$$C = p(\phi)C_S + p(1-\phi)C_L, \tag{1}$$

where the interpolation functions, $p(\phi) = p(\phi_S)$ and $p(1-\phi) = p(\phi_L)$, for solid (S) and liquid (L) phases,

respectively, are chosen to ensure a minimum of free energy density at $\phi = 0$ and $\phi = 1$ with $p(\phi) + p(1-\phi) = 1$ [30], $C_i$ ($i = S, L$) is the solute concentration in solid and liquid, and $\phi$ is the phase-field variable. In addition to the mixture of concentration in phases (1), the second kind constraint exists at any point in the bulk phases: $\phi_S + \phi_L = 1$ or $\boldsymbol{\nabla}\phi_S + \boldsymbol{\nabla}\phi_L = 0$ or $\partial\phi_S/\partial t + \partial\phi_L/\partial t = 0$.

In the subsequent theoretical investigations, we will evaluate the spatial and temporal derivatives of the phase-field variable, $\phi$, via interface thickness, velocity, and acceleration which are driven by the average force, $\Delta G$, and the interface curvature [28]. With this aim, we use the averaging method widely known in the mechanics of continuous media [31, 32] and in solidification processes [33, 34]. Particularly, Beckermann *et al* [35] used the volume or ensemble averaging methods that have been used to derive conservation equations for other multiphase systems [32, 36, 37]. Indeed, the $\phi$-variable can be formally related to the volume or ensemble average of an existence function $\chi_k$ for $k$th phase, which is unity in the solid and zero otherwise [32]

$$\phi = \phi_S = 1 - \phi_L = \frac{1}{\Delta v_0}\int_{\Delta v_0}\chi_S dv_0 = \langle\chi_S\rangle, \tag{2}$$

where the symbol $\langle...\rangle$ stands for an average over the volume $\Delta v_0$, which is macroscopically small [33, 37]. The average interfacial area, $\Delta A_i$, between the solid and liquid per unit volume is given by

$$\frac{\Delta A_i}{\Delta v_0} = \langle|\boldsymbol{\nabla}\chi_S|\rangle = |\boldsymbol{\nabla}\phi|. \tag{3}$$

Note that $\chi_k$ is dealt with as a generalized function, in particular, with regard to its differentiation such as

$$\boldsymbol{\nabla}\chi_k = \boldsymbol{n}_k\frac{\partial\chi_k}{\partial n}, \tag{4}$$

where $\boldsymbol{n}_k$ is the unit normal vector exterior to the $k$-th phase and $\partial\chi_k/\partial n$ is a scalar valued generalized function [32]. We assume, further, that the unit normal vector exterior to the solid phase $\boldsymbol{n}_S = \boldsymbol{n}$ and the exterior unit normal vector to the liquid phase $\boldsymbol{n}_L = -\boldsymbol{n}_S = -\boldsymbol{n}$ with the curvature takes the negative sign for the convex interfaces, $\kappa < 0$.

The definitions (2)–(4) yield the expression of the module of a phase-field gradient $|\boldsymbol{\nabla}\phi| = \partial\phi/\partial n$ and will be used to obtain the temporal and spatial derivatives of phase-field variable where the average unit normal vector exterior to the solid phase, $\boldsymbol{n}$, and the curvature, $\kappa$, of the solid-liquid interface are defined by (see [35] and references therein)

$$\boldsymbol{n} = -\frac{\boldsymbol{\nabla}\chi}{|\boldsymbol{\nabla}\chi|} = -\frac{\boldsymbol{\nabla}\phi}{|\boldsymbol{\nabla}\phi|}, \kappa = \boldsymbol{\nabla}\cdot\boldsymbol{n} = -\frac{1}{|\boldsymbol{\nabla}\phi|}\left[\boldsymbol{\nabla}^2\phi - \frac{(\boldsymbol{\nabla}\phi\cdot\boldsymbol{\nabla})|\boldsymbol{\nabla}\phi|}{|\boldsymbol{\nabla}\phi|}\right], \tag{5}$$

with

$$\frac{(\boldsymbol{\nabla}\phi\cdot\boldsymbol{\nabla})|\boldsymbol{\nabla}\phi|}{|\boldsymbol{\nabla}\phi|} = \frac{\partial^2\phi}{\partial n^2}. \tag{6}$$

Otherwise, the normal interface velocity $V = \boldsymbol{v}_i\cdot\boldsymbol{n}_L = -\boldsymbol{v}_i\cdot\boldsymbol{n}$ with the velocity of the interface $\boldsymbol{v}_i$ is given by

$$\boldsymbol{v}_i \cdot \boldsymbol{\nabla}\chi_k = -\frac{\partial \chi_k}{\partial t}, \qquad (7)$$

yields the first and second time derivative of $\phi$, respectively, as

$$\frac{\partial \phi}{\partial t} = -V\left|\boldsymbol{\nabla}\phi\right|, \qquad \frac{\partial^2 \phi}{\partial t^2} = -\mathcal{A}\left|\boldsymbol{\nabla}\phi\right| - V\frac{\partial\left(\left|\boldsymbol{\nabla}\phi\right|\right)}{\partial t}, \qquad (8)$$

where $\mathcal{A} = \partial V/\partial t$ stands for the interface acceleration (see [28] for more details of spatial and time derivatives of $\phi$).

It should be pointed out here that close to equilibrium, however, the model parameters can be related to physically measurable quantities like interfacial energy $\sigma$, interfacial mobility, deviation from thermodynamic equilibrium and the equilibrium interfacial width $\delta$ [19, 38]. These relations were derived from the one-dimensional steady-state solution of a traveling wave solution of the phase-field equation for three forms of the potential function: the so-called double-well, double-obstacle, and top-hat potentials (see appendix in [19]). Note that the notation of total free energy in the following theoretical background is chosen as in [19] to underline that the diffuse interface is treated as a volume with excess energy density $\sigma/\delta$.

## 3. Effective mobility approach to fast interfaces

The total free energy $\mathcal{G}$ in the entire volume $\Omega$ is

$$\mathcal{G} = \mathcal{G}^{\mathrm{e}} + \mathcal{G}^{\mathrm{ne}} = \int_\Omega \left(G^{\mathrm{e}}_{\mathrm{intf}} + G^{\mathrm{e}}_{\mathrm{bulk}} + G^{\mathrm{ne}}_{\mathrm{intf}} + G^{\mathrm{ad}}\right)\mathrm{d}\Omega, \qquad (9)$$

where the equilibrium contributions from the interface $G^{\mathrm{e}}_{\mathrm{intf}}$ and bulk phases $G^{\mathrm{e}}_{\mathrm{bulk}}$, non-equilibrium contribution from the interface $G^{\mathrm{ne}}_{\mathrm{intf}}$, and additional constraint $G^{\mathrm{ad}}$ are related to (1). The superscripts and the subscripts 'e', 'ne', 'intf', and 'bulk' denote the equilibrium, the non-equilibrium, the interface, and the bulk contributions, respectively.

### 3.1. The hodograph equation and traveling waves with the double-obstacle potential

In this case, the interpolation function takes the following form,

$$p(\phi) = \frac{\phi^2}{\phi^2 + (1-\phi)^2}, \qquad p(1-\phi) = \frac{(1-\phi)^2}{\phi^2 + (1-\phi)^2}, \qquad (10)$$

the double-obstacle function, $g(\phi)$, is written as

$$g(\phi) = \phi(1-\phi), \qquad (11)$$

and all contributions to the total free energy $\mathcal{G}$ are expressed as

$$G^{e}_{\mathrm{intf}} = \frac{4\sigma\delta}{\pi^2}(\boldsymbol{\nabla}\phi)^2 + \frac{4\sigma}{\delta}g(\phi), \qquad (12)$$

$$\begin{aligned} G^{\mathrm{e}}_{\mathrm{bulk}} &= \frac{1}{\upsilon_{\mathrm{m}}}(p(\phi)G_{\mathrm{S}} + p(1-\phi)G_{\mathrm{L}}) \\ &= \frac{1}{\upsilon_{\mathrm{m}}}\left[p(\phi)(C_{\mathrm{S}}\mu^{\mathrm{S}}_{\mathrm{A}} + (1-C_{\mathrm{S}})\mu^{\mathrm{S}}_{\mathrm{B}}) + p(1-\phi)(C_{\mathrm{L}}\mu^{L}_{\mathrm{A}} + (1-C_{\mathrm{L}})\mu^{L}_{\mathrm{B}})\right], \end{aligned} \qquad (13)$$

$$G^{\mathrm{ne}}_{\mathrm{intf}} = \frac{2\sigma\delta}{\pi^2(V^{\mathrm{B}}_\phi)^2}\left(\frac{\partial\phi}{\partial t}\right)^2, \qquad (14)$$

$$G^{\mathrm{ad}} = \lambda(p(\phi)C_{\mathrm{S}} + p(1-\phi)C_{\mathrm{L}} - C). \qquad (15)$$

Here $\sigma$ is the interface energy, $G^{\mathrm{e}}_{\mathrm{intf}}$ is defined as the double-obstacle potential [19] such that the interfacial width remains finite during solidification. $G^{\mathrm{e}}_{\mathrm{bulk}}$ is assumed to be a mixture of the molar Gibbs free energy $G_{\mathrm{S}}$ and $G_{\mathrm{L}}$ with $\mu^{i}_{j}$ the chemical potential ($i = S, L; j = A; B$) and, $G^{\mathrm{ad}}$ with the associated Lagrange multiplier $\lambda$ included into the total free energy $\mathcal{G}$ such that the solute conservation is ensured to describe the additional constraint (1) thermodynamically consistent. $\upsilon_m$ is the same assumed partial molar volume of solvent A and solute B, $\tilde{\mu}^i$ is the solute diffusion potential, $C_i$ is the concentration ($i = S, L$), $V^i_{\mathrm{D}}$ is the maximum solute diffusion speed in the bulk phases, $V^{\mathrm{B}}_\phi$ is the maximum phase-field propagation speed in bulk phases and $t$ is the time. The non-equilibrium contribution from interface $G^{\mathrm{ne}}_{\mathrm{intf}}$ is introduced due to extension of the set of 'slow' variables $\{C_{\mathrm{S}}, C_{\mathrm{L}}, \phi\}$ by the 'fast' variable, i.e. the gradient flow $\partial\phi/\partial t$ (the rate of change of the phase-field $\phi$) giving the full space of thermodynamic variables as $\{C_{\mathrm{S}}, C_{\mathrm{L}}, \phi, \partial\phi/\partial t\}$.

According to the thermodynamic extremal principle (TEP) [39, 40], the total free energy dissipation can be given as

$$Q = \int_\Omega \left[\frac{1}{M_\phi}\left(\frac{\partial\phi}{\partial t}\right)^2 + \left(\frac{1}{M^{\mathrm{Seff}}_{\mathrm{c}}}\boldsymbol{J}^{\mathrm{S2}}_{\mathrm{B}} + \frac{1}{M^{\mathrm{Leff}}_{\mathrm{c}}}\boldsymbol{J}^{\mathrm{L2}}_{\mathrm{B}}\right)\right]\mathrm{d}\Omega, \qquad (16)$$

with the phase-field propagation mobility, $M_\phi$, and effective mobilities for solute diffusion, $M^{\mathrm{Seff}}_{\mathrm{c}}$ and $M^{\mathrm{Leff}}_{\mathrm{c}}$, have respectively the following form [41],

$$M_\phi = \frac{\pi M\sqrt{\phi(1-\phi)}}{\delta(\partial p/\partial\phi)}, \qquad (17)$$

$$M^{\mathrm{ieff}}_{\mathrm{c}} = M^i_{\mathrm{c}}\left(1 + \frac{\upsilon_{\mathrm{m}}}{(V^i_{\mathrm{D}})^2}\frac{1}{\boldsymbol{\nabla}C_i}\frac{\partial\boldsymbol{J}^i_{\mathrm{B}}}{\partial t}\right), \qquad i = S, L \quad (18)$$

where $M$ is the mobility of interface migration and $M^i_{\mathrm{c}}$ is the mobility for equilibrium solute diffusion [41]. Therefore the evolution of the system follows from

$$\delta\left\{\frac{\mathrm{d}\mathcal{G}}{\mathrm{d}t} + \frac{Q}{2}\right\}_{\boldsymbol{J}^{\mathrm{S}}_{\mathrm{B}}, \boldsymbol{J}^{\mathrm{L}}_{\mathrm{B}}, \frac{\partial\phi}{\partial t}} = 0, \qquad (19)$$

where $\mathcal{G}$ is given by (9).

Eliminating the associated Lagrange multiplier $\lambda$ in (19) yields equations of the phase-field model for fast and slow dynamics,

$$\left\{\begin{matrix} \frac{\partial\phi}{\partial t} \\ \boldsymbol{J}^{\mathrm{S}}_{\mathrm{B}} \\ \boldsymbol{J}^{\mathrm{L}}_{\mathrm{B}} \end{matrix}\right\} = \begin{bmatrix} \boldsymbol{L}_{\phi\phi} & \boldsymbol{L}_{\phi\mathrm{C_S}} & \boldsymbol{L}_{\phi\mathrm{C_L}} \\ \boldsymbol{L}_{\mathrm{C_S}\phi} & L_{\mathrm{C_S}\mathrm{C_S}} & L_{\mathrm{C_S}\mathrm{C_L}} \\ \boldsymbol{L}_{\mathrm{C_L}\phi} & L_{\mathrm{C_L}\mathrm{C_S}} & L_{\mathrm{C_L}\mathrm{C_L}} \end{bmatrix} \left\{\begin{matrix} \frac{\delta\mathcal{G}}{\delta\phi} \\ \upsilon_{\mathrm{m}}\boldsymbol{\nabla}\frac{\delta\mathcal{G}}{\delta C_{\mathrm{S}}} \\ \upsilon_{\mathrm{m}}\boldsymbol{\nabla}\frac{\delta\mathcal{G}}{\delta C_{\mathrm{L}}} \end{matrix}\right\}, \quad (20)$$

where

$$\frac{\delta\mathcal{G}}{\delta\phi} = -\frac{8\sigma\delta}{\pi^2}\boldsymbol{\nabla}^2\phi + \frac{4\sigma}{\delta}\frac{\partial g(\phi)}{\partial\phi} + \frac{8\sigma\delta}{\pi^2(V^{\mathrm{B}}_\phi)^2}\frac{\partial^2\phi}{\partial t^2} + \frac{(G_S - G_L)}{\upsilon_{\mathrm{m}}}\frac{\partial p(\phi)}{\partial\phi}, \qquad (21)$$

$$\frac{\delta \mathcal{G}}{\delta C_S} = \frac{p(\phi)(\mu_B^S - \mu_A^S)}{\upsilon_m} = \frac{p(\phi)\tilde{\mu}^S}{\upsilon_m}, \qquad (22)$$

$$\frac{\delta \mathcal{G}}{\delta C_L} = \frac{p(1-\phi)(\mu_B^L - \mu_A^L)}{\upsilon_m} = \frac{p(1-\phi)\tilde{\mu}^L}{\upsilon_m}, \qquad (23)$$

and the detailed expressions of the kinetic coefficients, $L_{m_1 m_2}$ ($m_1, m_2 = \phi, C_S, C_L$), are given in [27]. Then, the evolution equation follows from (20) as

$$\frac{1}{M_\phi}\frac{\partial \phi}{\partial t} = -\frac{\delta \mathcal{G}}{\delta \phi} + \frac{1}{2}\frac{1}{\upsilon_m}\frac{\partial p}{\partial \phi}\frac{(C_S - C_L)}{\boldsymbol{\nabla} p}$$
$$\times \left( \frac{\boldsymbol{J}_B^S}{M_c^{Seff}} - \frac{\boldsymbol{J}_B^L}{M_c^{Leff}} + \upsilon_m \boldsymbol{\nabla}\frac{\delta \mathcal{G}}{\delta C_S} - \upsilon_m \boldsymbol{\nabla}\frac{\delta \mathcal{G}}{\delta C_L} \right), \qquad (24)$$

with

$$\frac{\boldsymbol{J}_B^S}{M_c^{Seff}} + \frac{\boldsymbol{J}_B^L}{M_c^{Leff}} + \upsilon_m \boldsymbol{\nabla}\frac{\delta \mathcal{G}}{\delta C_S} + \upsilon_m \boldsymbol{\nabla}\frac{\delta \mathcal{G}}{\delta C_L} = 0, \qquad (25)$$

$$\boldsymbol{J}_B^S - \boldsymbol{J}_B^L = -\frac{1}{\upsilon_m}\frac{(C_S - C_L)}{\boldsymbol{\nabla}\phi}\frac{\partial \phi}{\partial t}. \qquad (26)$$

Taking into account (21) with (11), one can obtain from (24) the following equation for the phase-field $\phi$:

$$\tau_\phi \frac{\partial^2 \phi}{\partial t^2} + \frac{\partial \phi}{\partial t} = M_\phi \left( \frac{8\sigma\delta}{\pi^2}\boldsymbol{\nabla}^2\phi - \frac{4\sigma}{\delta}(1-2\phi) - \Delta G\frac{\partial p}{\partial \phi} \right), \qquad (27)$$

with

$$\Delta G = \Delta G^e + \Delta G^{ne}, \qquad (28)$$

$$\Delta G^e = \frac{G_S - G_L}{\upsilon_m}, \qquad (29)$$

$$\Delta G^{ne} = -\frac{1}{2}\frac{1}{\upsilon_m}\frac{(C_S - C_L)}{\boldsymbol{\nabla} p}\left( \frac{\boldsymbol{J}_B^S}{M_c^{Seff}} - \frac{\boldsymbol{J}_B^L}{M_c^{Leff}} + \upsilon_m \boldsymbol{\nabla}\frac{\delta \mathcal{G}}{\delta C_S} - \upsilon_m \boldsymbol{\nabla}\frac{\delta \mathcal{G}}{\delta C_L} \right), \qquad (30)$$

$$\tau_\phi = \frac{8M\sigma}{\pi(V_\phi^B)^2}\frac{\sqrt{\phi(1-\phi)}}{(\partial p/\partial \phi)}, \qquad (31)$$

where $\Delta G$ stands for the total driving free energy from the bulk contribution reformulated into the molar driving free energy, $\Delta G^e$, the equilibrium and the non-equilibrium bulk contributions, $\Delta G^{ne}$, and $\tau_\phi$ is the relaxation time of the gradient flow.

Using the same treatment as in [28], one obtains from (2)–(8) the spatial and time derivatives of the phase-field with the following traveling wave profile of the phase-field

$$\phi(n,t) = \begin{cases} 0 & \frac{n}{\ell(t)} < -\frac{\pi}{2} \\ \frac{1}{2}\left[ 1 + \sin\left( \frac{n}{\ell(t)} \right) \right] & -\frac{\pi}{2} \leqslant \frac{n}{\ell(t)} < \frac{\pi}{2} \\ 1 & \frac{n}{\ell(t)} \geqslant \frac{\pi}{2}, \end{cases} \qquad (32)$$

where $\ell = \ell(t)$ stands for the time-dependent effective width of the interface and $n$ is the spatial coordinate normal to the interface. Therefore, one gets

$$\boldsymbol{\nabla}^2\phi = -\kappa\frac{\sqrt{\phi(1-\phi)}}{\ell} + \frac{(1-2\phi)}{2\ell^2}, \qquad (33)$$

$$\frac{\partial \phi}{\partial t} = -V\frac{\sqrt{\phi(1-\phi)}}{\ell}, \qquad (34)$$

$$\frac{\partial^2 \phi}{\partial t^2} = -\left( \mathcal{A} - \frac{V}{\ell}\frac{\partial \ell}{\partial t} \right)\frac{\sqrt{\phi(1-\phi)}}{\ell} + V^2\frac{(1-2\phi)}{2\ell^2}, \qquad (35)$$

with

$$V\frac{\partial(|\boldsymbol{\nabla}\phi|)}{\partial t} = -\frac{V}{\ell}\frac{\partial \ell}{\partial t}\frac{\sqrt{\phi(1-\phi)}}{\ell} - V^2\frac{(1-2\phi)}{2\ell^2}. \qquad (36)$$

Taking into account (17) and substituting (33)–(36) into (27), one finds the following nonlinear equation,

$$0 = \left\{ \left[ \tau_\phi\left( \mathcal{A} - \frac{V}{\ell}\frac{\partial \ell}{\partial t} \right) + V - \frac{8\sigma\delta M_\phi}{\pi^2}\kappa \right]\frac{1}{\ell} - \frac{\pi M}{\delta}\Delta G \right\}\sqrt{\phi(1-\phi)}$$
$$+ \left[ \left( \frac{8\sigma\delta}{\pi^2} - \frac{\tau_\phi}{M_\phi}V^2 \right)\frac{M_\phi}{2\ell^2} - \frac{4\sigma M_\phi}{\delta} \right](1-2\phi), \qquad (37)$$

which can be solved by accepting zero values for expressions in the curly brackets (the first term) and the square brackets (the second term). Using (17) and (31), the expression for the interface width $\ell$ follows from the second term in square brackets in right-hand side of (37) as

$$\ell(t) = \frac{\delta}{\pi}\sqrt{1 - V^2(t)/(V_\phi^B)^2}, \quad V(t) < V_\phi^B. \qquad (38)$$

In (38) and in the following text we assume that the interface velocity $V(t)$ cannot overcome the maximum speed $V_\phi^B$ of the phase-field propagation because the interface cannot be faster than the field in which this interface moves.

Using the expression for interface width (38), the expression $(V/\ell)(\partial \ell/\partial t)$ from (37) takes the form

$$\frac{V}{\ell}\frac{\partial \ell}{\partial t} = -\frac{\mathcal{A}\left[ V^2(t)/(V_\phi^B)^2 \right]}{1 - V^2(t)/(V_\phi^B)^2}. \qquad (39)$$

The first term in curly brackets in right-hand side of (37) with (17) and (31) gives the following hodograph equation,

$$\frac{\tau_\phi \mathcal{A}}{\left[ 1 - V^2(t)/(V_\phi^B)^2 \right]^{3/2}} + \frac{V}{\sqrt{1 - V^2(t)/(V_\phi^B)^2}} = M\Delta G + \frac{[\tau_\phi(V_\phi^B)^2]\kappa}{\sqrt{1 - V^2(t)/(V_\phi^B)^2}}. \qquad (40)$$

### 3.2. The hodograph equation and traveling waves with the double-well potential

Choosing the interpolation function as

$$p(\phi) = \phi^2(3 - 2\phi), \qquad p(1-\phi) = (1-\phi)^2(3 - 2(1-\phi)), \qquad (41)$$

and using the double-well function $g(\phi)$ of the following form

$$g(\phi) = \phi^2(1-\phi)^2, \qquad (42)$$

the equilibrium and non-equilibrium contributions from the interface, $G_{intf}^e$ and $G_{intf}^{ne}$, to the total free energy $\mathcal{G}$ become, respectively,

$$G_{\text{intf}}^{\text{e}} = \frac{\sigma\delta}{2}(\boldsymbol{\nabla}\phi)^2 + \frac{9}{2}\frac{\sigma}{\delta}g(\phi), \qquad (43)$$

$$G_{\text{intf}}^{\text{ne}} = \frac{1}{2}\frac{\sigma\delta}{(V_\phi^{\text{B}})^2}\left(\frac{\partial\phi}{\partial t}\right)^2, \qquad (44)$$

where the contribution from the interface energy, $G_{\text{intf}}^{\text{e}}$, is defined as the double-well potential [19] such that the interfacial width remains finite upon solidification. The equilibrium contribution to bulk phases, $G_{\text{bulk}}^{\text{e}}$ and additional constraint $G^{\text{ad}}$ to the total free energy $\mathcal{G}$ remain unchanged (they are given by (13) and (15), respectively).

Based on the TEP (see (16) and (19)), the system of equation (20) yields almost the same governing equation of the phase-field (24)–(26), with

$$\frac{\delta\mathcal{G}}{\delta\phi} = -\sigma\delta\boldsymbol{\nabla}^2\phi + \frac{9\sigma}{2\delta}\frac{\partial g(\phi)}{\partial\phi} + \frac{\sigma\delta}{(V_\phi^{\text{B}})^2}\frac{\partial^2\phi}{\partial t^2} + \frac{1}{2}\frac{G_{\text{S}} - G_{\text{L}}}{v_{\text{m}}}\frac{\partial p}{\partial\phi}, \qquad (45)$$

and the phase-field propagation mobility, $M_\phi$, takes the following form

$$M_\phi = \frac{M\nabla\phi}{\partial p/\partial\phi}. \qquad (46)$$

Taking into account (41), (42) and (45), the governing equation of the phase-field (24) becomes

$$\tau_\phi\frac{\partial^2\phi}{\partial t^2} + \frac{\partial\phi}{\partial t} = M_\phi\left[\sigma\delta\boldsymbol{\nabla}^2\phi - \frac{9\sigma}{\delta}\phi(1-\phi)(1-2\phi) - 3\Delta G\phi(1-\phi)\right], \qquad (47)$$

where the relaxation time $\tau_\phi$ takes the form

$$\tau_\phi = \frac{\sigma\delta}{(V_\phi^{\text{B}})^2}M_\phi. \qquad (48)$$

Using (2)–(8) for the spatial and time derivatives of the phase-field one can find that the phase-field propagates as

$$\phi(n, t) = \frac{1}{2}\left[1 + \tanh\left(\frac{n}{\ell(t)}\right)\right], \qquad (49)$$

where $\ell = \ell(t)$ stands for the time-dependent width of the interface and $n$ is the spatial coordinate normal to the interface. Therefore, one gets in the case of double-well potential,

$$\boldsymbol{\nabla}^2\phi = -\kappa\frac{2\phi(1-\phi)}{\ell} + \frac{4\phi(1-\phi)(1-2\phi)}{\ell^2}, \qquad (50)$$

$$\frac{\partial\phi}{\partial t} = -V\left(\frac{2\phi(1-\phi)}{\ell}\right), \qquad (51)$$

$$\frac{\partial^2\phi}{\partial t^2} = -\left(\mathcal{A} - \frac{V}{\ell}\frac{\partial\ell}{\partial t}\right)\frac{2\phi(1-\phi)}{\ell} + V^2\frac{4\phi(1-\phi)(1-2\phi)}{\ell^2}, \qquad (52)$$

with

$$V\frac{\partial(|\boldsymbol{\nabla}\phi|)}{\partial t} = -\frac{V}{\ell}\frac{\partial\ell}{\partial t}\frac{2\phi(1-\phi)}{\ell} - V^2\frac{4\phi(1-\phi)(1-2\phi)}{\ell^2}. \qquad (53)$$

Substituting (50)–(52) in (47) and taking into account (46), one finds the equation

$$0 = \left\{\left[\tau_\phi\left(\mathcal{A} - \frac{V}{\ell}\frac{\partial\ell}{\partial t}\right) + V - M_\phi\sigma\delta\kappa\right]\frac{2}{\ell} - 3\Delta GM_\phi\right\}\phi(1-\phi)$$
$$+ \left[(M_\phi\sigma\delta - \tau_\phi V^2)\frac{4}{\ell^2} - 9\frac{M_\phi\sigma}{\delta}\right]\phi(1-\phi)(1-2\phi), \qquad (54)$$

which can be solved by accepting zero values for expressions in the curly brackets (the first term) and the square brackets (the second term).

Taking into account (48), the expression for the velocity-dependent interface width $\ell$ follows from the second term in square brackets in right-hand side of (54) as

$$\ell(t) = \frac{2}{3}\delta\sqrt{1 - V^2(t)/(V_\phi^{\text{B}})^2}, \quad V(t) < V_\phi^{\text{B}}. \qquad (55)$$

Now, using the interface width (55) one can derive the same expression as (39), which appears in the first term of right-hand side of (54). Therefore, the first term in curly brackets in right-hand side of (54) with (48) gives the following hodograph equation,

$$\frac{\tau_\phi\,\mathcal{A}}{\left[1 - V^2(t)/(V_\phi^{\text{B}})^2\right]^{3/2}} + \frac{V}{\sqrt{1 - V^2(t)/(V_\phi^{\text{B}})^2}}$$
$$= \frac{[\tau_\phi(V_\phi^{\text{B}})^2]}{\sigma}\Delta G + \frac{[\tau_\phi(V_\phi^{\text{B}})^2]\kappa}{\sqrt{1 - V^2(t)/(V_\phi^{\text{B}})^2}}. \qquad (56)$$

## 4. Kinetic energy approach to fast interfaces

The kinetic energy approach [25, 26] introduces the total free energy $\mathcal{G}$ consisting of the equilibrium and the non-equilibrium contributions using the set of 'slow' variables $\{C_{\text{S}}, C_{\text{L}}, \phi\}$ and the space of 'fast' variables $\{\boldsymbol{J}_{\text{B}}^{\text{S}}, \boldsymbol{J}_{\text{B}}^{\text{L}}, \partial\phi/\partial t\}$. Here we deal with the case of the traveling wave solution with the double-obstacle potential for a binary alloy system consisting of A-atoms (solvent) together with B-atoms (solute) under constant temperature $T$ and constant pressure.

### 4.1. The hodograph equation and traveling waves with the double-obstacle potential

The total free energy $\mathcal{G}$ in the entire volume $\Omega$ is written as

$$\mathcal{G} = \mathcal{G}^{\text{e}} + \mathcal{G}^{\text{ne}} = \int_\Omega (G_{\text{intf}}^{\text{e}} + G_{\text{bulk}}^{\text{e}} + G_{\text{intf}}^{\text{ne}} + G_{\text{bulk}}^{\text{ne}})\,\text{d}\Omega. \qquad (57)$$

The non-equilibrium contribution from bulk phases, $G_{\text{bulk}}^{\text{ne}}$, related to the fast variables, $\boldsymbol{J}_{\text{B}}^{\text{S}}$ and $\boldsymbol{J}_{\text{B}}^{\text{L}}$, is given by

$$G_{\text{bulk}}^{\text{ne}} = \frac{1}{v_{\text{m}}}\left(p(\phi)\frac{1}{2}\alpha_{\text{S}}\boldsymbol{J}_{\text{B}}^{\text{S2}} + p(1-\phi)\frac{1}{2}\alpha_{\text{L}}\boldsymbol{J}_{\text{B}}^{\text{L2}}\right). \qquad (58)$$

The expression (57) contains the same equilibrium and non-equilibrium contributions from the interface, $G_{\text{intf}}^{\text{e}}$ and $G_{\text{intf}}^{\text{ne}}$, and the same equilibrium contrubution from bulk phases, $G_{\text{bulk}}^{\text{e}}$, as in the effective mobility approach for the case of double-obstacle potential, (12)–(14), where $\alpha_i = (\partial\tilde{\mu}^i/\partial C_i)\,v_{\text{m}}^2/V_{\text{D}}^{i2}$ the positive kinetic coefficient independent from the solute

flux $\boldsymbol{J}_B^i$ [26]. The additional constraints in the modeling system are defined by (i) the single-phase state at any point in the bulk phases [27], i.e. $\phi_S + \phi_L = 1$ or $\boldsymbol{\nabla}\phi_S + \boldsymbol{\nabla}\phi_L = 0$ or $(\partial\phi_S/\partial t) + (\partial\phi_L/\partial t) = 0$ and (ii) the mixture law (1), i.e. C is a mixture of $C_S$ and $C_L$.

According to the TEP [39, 40], the total free energy dissipation can be given as

$$Q = \int_\Omega \left[ \frac{1}{M_\phi}\left(\frac{\partial\phi}{\partial t}\right)^2 + \left(\frac{1}{M_c^S}\boldsymbol{J}_B^{S2} + \frac{1}{M_c^L}\boldsymbol{J}_B^{L2}\right) \right] d\Omega, \qquad (59)$$

with the phase-field propagation mobility, $M_\phi$, and solute diffusion mobilities, $M_c^S$ and $M_c^L$, have respectively the following form [41],

$$M_\phi = \frac{\pi M \sqrt{\phi(1-\phi)}}{\delta(\partial p/\partial\phi)}, \qquad (60)$$

$$M_c^S = \frac{pD_S}{v_m}\left(\frac{\partial\tilde{\mu}^S}{\partial C_S}\right)^{-1}, \qquad (61)$$

$$M_c^L = \frac{(1-p)D_L}{v_m}\left(\frac{\partial\tilde{\mu}^L}{\partial C_L}\right)^{-1}, \qquad (62)$$

where $M$ is the mobility of interface migration and $D_i$ is the solute diffusion coefficient. Therefore, the evolution of the system follows from the variational derivative

$$\delta\left\{\frac{d\mathcal{G}}{dt} + \frac{Q}{2} + \lambda\int_\Omega\left[(\boldsymbol{J}_B^S - \boldsymbol{J}_B^L)v_m\boldsymbol{\nabla}\phi + \frac{\partial\phi}{\partial t}(C_S - C_L)\right]d\Omega\right\}_{\boldsymbol{J}_B^S\boldsymbol{J}_B^L,\frac{\partial\phi}{\partial t}} = 0, \qquad (63)$$

where $\lambda$ is the associated Lagrange multiplier and the time derivative $d\mathcal{G}/dt$ should be taken from the total free energy (57).

Eliminating $\lambda$ in (63) yields the system of equations of the phase-field model for fast and slow dynamics,

$$\begin{Bmatrix}\frac{\partial\phi}{\partial t}\\ \boldsymbol{J}_B^S\\ \boldsymbol{J}_B^L\end{Bmatrix} = \begin{bmatrix}\boldsymbol{L}_{\phi\phi} & \boldsymbol{L}_{\phi c_S} & \boldsymbol{L}_{\phi c_L}\\ \boldsymbol{L}_{c_S\phi} & \boldsymbol{L}_{c_S c_S} & \boldsymbol{L}_{c_S c_L}\\ \boldsymbol{L}_{c_L\phi} & \boldsymbol{L}_{c_L c_S} & \boldsymbol{L}_{c_L c_L}\end{bmatrix}\begin{Bmatrix}\frac{\delta\mathcal{G}}{\delta\phi} + \frac{\partial p(\phi)}{\partial\phi}\frac{1}{v_m}\left(\frac{1}{2}\alpha_S\boldsymbol{J}_B^{S2} - \frac{1}{2}\alpha_L\boldsymbol{J}_B^{L2}\right)\\ v_m\boldsymbol{\nabla}\frac{\delta\mathcal{G}}{\delta C_S} + \frac{p(\phi)\alpha_S}{v_m}\frac{\partial\boldsymbol{J}_B^S}{\partial t}\\ v_m\boldsymbol{\nabla}\frac{\delta\mathcal{G}}{\delta C_L} + \frac{p(1-\phi)\alpha_L}{v_m}\frac{\partial\boldsymbol{J}_B^L}{\partial t}\end{Bmatrix}, \qquad (64)$$

where $L_{m_1 m_2}$ $(m_1, m_2 = \phi, C_S, C_L)$ are the kinetic coefficients given in [27]. Then, the equation of the phase-field $\phi$ follows from (64) as

$$\tau_\phi\frac{\partial^2\phi}{\partial t^2} + \frac{\partial\phi}{\partial t} = -M_\phi\left\{\frac{4\sigma}{\delta}\left[-\frac{2\delta^2}{\pi^2}\boldsymbol{\nabla}^2\phi + (1-2\phi)\right] + \Delta G\frac{\partial p}{\partial\phi}\right\}, \qquad (65)$$

where $\Delta G = \Delta G^e + \Delta G^{ne}$ stands for the total driving free energy from the bulk contribution reformulated into the molar driving free energy, $\Delta G^e$, the equilibrium and the non-equilibrium bulk contributions, $\Delta G^{ne}$. The relaxation time is

$$\tau_\phi = \frac{8M\sigma}{\pi(V_\phi^B)^2}\frac{\sqrt{\phi(1-\phi)}}{\partial p/\partial\phi}. \qquad (66)$$

Introducing now the spatial and time derivatives of the phase-field from (33)–(36) into (65) and taking into account (60), one finds the equation

$$0 = \left\{\left(\tau_\phi\left[\mathcal{A} - \frac{V}{\ell}\frac{\partial\ell}{\partial t}\right] + V - \frac{8\sigma\delta M_\phi}{\pi^2}\kappa\right)\frac{1}{\ell} - \frac{\pi M}{\delta}\Delta G\right\}\sqrt{\phi(1-\phi)}$$
$$+ \left[\left(\frac{8\sigma\delta}{\pi^2} - \frac{\tau_\phi}{M_\phi}V^2\right)\frac{M_\phi}{2\ell^2} - \frac{4\sigma M_\phi}{\delta}\right](1-2\phi), \qquad (67)$$

which can be solved by accepting zero values for expressions in the curly brackets (the first term) and the square brackets (the second term).

Taking into account (60) and (66), the expression for the interface width (38) follows from the second term in square brackets in right-hand side of (67). The hodograph equation comes from the curly brackets of (67), which has the form of (40).

### 4.2. The hodograph equation and traveling waves with the double-well potential

Under the assumption of constant averaged driving force, $\Delta G$, a sole equation of the phase-field with the driving force, which is given by deviations of temperature and concentration from their equilibrium values within the diffuse interface, appeared from the equations for the hyperbolic transport and fast interface dynamics (see the work [28] and references therein)

$$\tau_\phi\frac{\partial^2\phi}{\partial t^2} + \frac{\partial\phi}{\partial t} = \nu\left[\nabla^2\phi - \frac{9}{2\delta^2}\frac{dg(\phi)}{d\phi} - \frac{1}{2\sigma\delta}\Delta G\frac{dp(\phi)}{d\phi}\right], \qquad (68)$$

where the interpolation function $p(\phi)$ and the double-well function $g(\phi)$ are given by (41) and (42), respectively, and the model parameters are expressed in terms of the surface energy $\sigma$, the interfacial width $\delta$, and the phase-field diffusion parameter $\nu$ are

$$M_\phi = \frac{\nu}{2\sigma\delta}, \qquad\qquad \tau_\phi = \frac{\nu}{(V_\phi^B)^2}. \qquad (69)$$

Substituting the spatial and time derivatives (50)–(52) into (68) gives the equation

$$0 = \left[(\nu - \tau_\phi V^2)\frac{4}{\ell^2} - 9\frac{\nu}{\delta^2}\right]\phi(1-\phi)(1-2\phi)$$
$$+ \left\{\frac{2}{\ell}\left[\tau_\phi\left(\mathcal{A} - \frac{V}{\ell}\frac{\partial\ell}{\partial t}\right) + V - \nu\kappa\right] - 3\frac{\nu}{\sigma\delta}\Delta G\right\}\phi(1-\phi), \qquad (70)$$

which can be solved by accepting zero values for expressions in the square brackets (the first term) and the curly brackets (the second term). Taking into account (69), the expression (55) for the interface width follows from the first term in square brackets in right-hand side of (70) as well as the hodograph equation (56) is obtained from the second term in curly brackets [28].

## 5. Summary on theoretical treatments

In summary of sections 3 and 4, effective mobility and kinetic energy approaches yield the same expressions of the velocity-dependent interface width $\ell(t)$ and hodograph equation with respect to the considered form of the phase-field profile $\phi(n, t)$

**Table 1.** Comparison of the main functions and coefficients within effective mobility approach (EMA) and kinetic energy approach (KEA).

| Function/Coefficient | Double-obstacle potential | Double-well potential | |
|---|---|---|---|
| Phase-field profile, $\phi(n,t)$ | $\begin{cases} 0 & \frac{n}{\ell(t)} < -\frac{\pi}{2} \\ \frac{1}{2}[1 + \sin(\frac{n}{\ell(t)})] & -\frac{\pi}{2} \leqslant \frac{n}{\ell(t)} < \frac{\pi}{2} \\ 1 & \frac{n}{\ell(t)} \geqslant \frac{\pi}{2} \end{cases}$ | $\frac{1}{2}[1 + \tanh(\frac{n}{\ell(t)})]$ | |
| Potential with energetic barrier, $g(\phi)$ | $\phi(1-\phi)$ | $\phi^2(1-\phi)^2$ | |
| Interpolation function, $p(\phi)$ | $\phi^2/(\phi^2 + (1-\phi)^2)$ | $\phi^2(3-2\phi)$ | |
| | EMA and KEA | EMA | KEA |
| Diffuse interface width, $\eta_{\text{int}}$ | $\delta/\pi$ | $2\delta/3$ | $2\delta/3$ |
| Mobility of interface migration, $\mathcal{M}$ | $M$ | $\tau_\phi(V_\phi^{\text{B}})^2/\sigma$ | $\nu/\sigma$ |
| Mobility of $\phi$-propagation, $M_\phi$ | $(\frac{\pi}{2})^2[\tau_\phi(V_\phi^{\text{B}})^2/(2\sigma\delta)]$ | $\tau_\phi(V_\phi^{\text{B}})^2/(\sigma\delta)$ | $\nu/(2\sigma\delta)$ |
| Relaxation time of gradient flow, $\tau_\phi$ | $\frac{8}{\pi}\frac{\sigma M}{(V_\phi^{\text{B}})^2}\frac{\sqrt{\phi(1-\phi)}}{\partial p/\partial\phi}$ | $\frac{\sigma M}{(V_\phi^{\text{B}})^2}\frac{\delta\nabla\phi}{\partial p/\partial\phi}$ | $\nu/(V_\phi^{\text{B}})^2$ |

in the dynamical regime. Using double-well and double-obstacle potentials, the unified interface width takes the form,

$$\ell(t) = \eta_{\text{int}}\sqrt{1 - V^2(t)/(V_\phi^{\text{B}})^2}, \quad V(t) < V_\phi^{\text{B}}, \quad (71)$$

and the unified hodograph equation can be written as

$$\frac{\tau_\phi\,\mathcal{A}}{\left[1 - V^2(t)/(V_\phi^{\text{B}})^2\right]^{3/2}} + \frac{V}{\sqrt{1 - V^2(t)/(V_\phi^{\text{B}})^2}} = \mathcal{M}\Delta\mathbb{G} + \frac{[\tau_\phi(V_\phi^{\text{B}})^2]\,\kappa}{\sqrt{1 - V^2(t)/(V_\phi^{\text{B}})^2}}, \quad (72)$$

where $\Delta\mathbb{G}$ stands for the unified driving force, $\eta_{\text{int}}$ and $\mathcal{M}$ are the unified interfacial width and unified interface migration mobility, respectively. Comparison between the obtained relations for $\eta_{\text{int}}$ and $\mathcal{M}$ as well as for the relaxation time, $\tau_\phi$, and phase-field propagation mobility, $M_\phi$, are given in table 1 with respect to double-well and double-obstacle potentials with using effective mobility approach (EMA) and kinetic energy approach (KEA).

## 6. Comparison with data of atomistic simulation

Previously, the nonlinearity in the growth kinetics of a form of the velocity with saturation has been described for pure Ni [28, 42]. However, there are other type of non-linearity in the 'velocity–undercooling' relationship which is presented by the crystal growth velocity curve having a maximum at fixed undercooling [29, 43, 44] typical for glass-forming metals and alloys. Because *in situ* measurements of kinetic phenomena at the solid-liquid interface are still experimentally inaccessible for metallic and semiconductor melts, the hodograph equation (72) is quantitatively tested in this section in comparison with the data of atomistic simulation. For such comparison, we choose the data obtained by Tang and Harrowell [29] in a molecular dynamics simulation of crystallization of undercooled $Cu_{50}Zr_{50}$ melts. These authors studied the growth kinetics of crystals in the steady-state regime with the constant velocity $V$ and with the absence of acceleration, $\mathcal{A} = 0$. Therefore, using approximations summarized in [45] and taking into account that $Cu_{50}Zr_{50}$ is the congruently melting alloy solidifying without chemical segregation, the hodograph equation (72) can be rewritten as

$$V = \frac{\mu_{\text{k}}(\Delta T_{\text{k}})\Delta T_{\text{k}}}{\sqrt{1 + \left[\mu_{\text{k}}(\Delta T_{\text{k}})\Delta T_{\text{k}}/V_\phi^{\text{B}}(\Delta T_{\text{k}})\right]^2}}, \quad (73)$$

where $\mu_{\text{k}}$ is the kinetic coefficient dependent on the kinetic undercooling $\Delta T_{\text{k}}$.

As predicted from (73), the interface velocity is proportional to the undercooling, $V \propto \Delta T_{\text{k}}$, giving the linear dependence at the small undercooling. With the increase of undercooling, the square root in denominator of (73) becomes more and more significant that leads to the nonlinearity and decreasing of the velocity. This denominator appears as the result of the relaxation of the gradient flow $\partial\phi/\partial t$ [45] and the contribution of the square root becomes essential at the high undercooling. This is obvious because $\partial\phi/\partial t$ has been introduced as the independent thermodynamic variable due to appearance of large driving forces on crystallization.

Substituting (73) into interfacial width (71) gives

$$\ell = \frac{\eta_{int}}{\sqrt{1 + \left(\mathcal{M}\Delta\mathbb{G}/V_\phi^B\right)^2}}. \quad (74)$$

In the local equilibrium limit, $V_\phi^{\text{B}} \to \infty$, i.e. with the instant relaxation of the gradient flow, $\tau \to 0$ (see expressions of Set 1 of table 2), the interfacial width (74) takes its equilibrium value $\ell = \eta_{int}$. With the increasing driving force $\Delta\mathbb{G}$, the diffuse interface shrinks and, with its largest value, $\Delta\mathbb{G} \to \infty$, the diffuse interface transforms to the sharp interface having the zero width, $\ell \to 0$.

In (73), the kinetic coefficient $\mu_{\text{k}}$ depends on the undercooling $\Delta T_{\text{k}}$ as

$$\mu_{\text{k}}(\Delta T_{\text{k}}) = \frac{D_\phi(\Delta T_{\text{k}})\Delta H_{\text{f}}}{\sigma T_{\text{m}}}, \quad (75)$$

where $\Delta H_{\text{f}}$ is the enthalpy of fusion. The maximum speed $V_\phi^{\text{B}}$ of the phase-field propagation is defined in (73) by the diffusion coefficient $D_\phi$ of the phase-field and relaxation time $\tau_\phi$ of the gradient flow as

$$V_\phi^{\text{B}}(\Delta T_{\text{k}}) = \sqrt{D_\phi(\Delta T_{\text{k}})/\tau_\phi}, \quad (76)$$

**Table 2.** Material parameters of glass-forming alloy $Cu_{50}Zr_{50}$ used in calculations.

| Parameter | Set 1 | Set 2 | Source |
|---|---|---|---|
| Melting temperature, $T_m$ (K), | 1340 | 1340 | [29] |
| Pseudo-glass temperature, $T_{AB}$ (K), | 940 | 940 | [46] |
| Interface energy, $\sigma$ (J m$^{-2}$), | 0.6 | 0.6 | [47] |
| Enthalpy of fusion, $\Delta H_f$ (J m$^{-3}$), | $8.78 \times 10^8$ | $8.78 \times 10^8$ | [47] |
| Relaxation time of gradient flow, $\tau_\phi$ (s), | $\to 0$ | $2.34 \times 10^{-8}$ | Present work |
| Diffusion factor, $D_\phi^0$ (m$^2$ s$^{-1}$), | $1.55 \times 10^{-9}$ | $1.55 \times 10^{-9}$ | Present work |
| Energetic barrier, $E_A$ (K), | 82.02 | 82.02 | Present work |
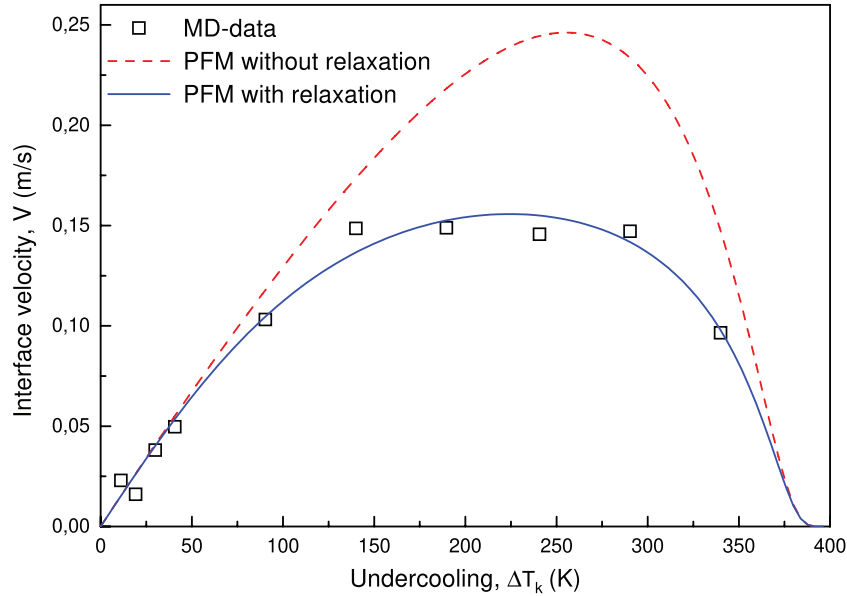


**Figure 1.** Data of molecular dynamic simulation ($\square$) obtained for the $\langle 100 \rangle$-direction of crystals growing from the undercooled glass-forming $Cu_{50}Zr_{50}$ alloy melt [29] in comparison with predictions of equations (73)–(77) given by the phase-field model (PFM) (curves). Calculations are given by: ($\boldsymbol{- - -}$) without relaxation of the gradient flow, $\tau_\phi \to 0$, $V_\phi^B \to \infty$, using Set 1 from table 2; (——) with relaxation, $\tau_\phi \neq 0$, finite $V_\phi^B$ and the parameters given by Set 2 from table 2.

where the relaxation time $\tau_\phi$ is taken as an independent parameter from the temperature in the present analysis. The diffusion coefficient of phase-field in (75) and (76) is

$$D_\phi(\Delta T_k) = D_\phi^0 \exp\left(-\frac{E_A}{T_m - \Delta T_k - T_{AB}}\right), \quad (77)$$

where the diffusion factor $D_\phi^0$, the energetic barrier $E_A$ and the pseudo-glass transition temperature $T_{AB}$ are the parameters of the phase-field propagation. As soon as the undercooling approaches its critical value in (77), the phase-field diffusion begins its steep decrease down to the zero value [45]. Finally, the kinetic equation (73) with (75)–(77) have previously been applied to describe the molecular simulation data on crystallization of Fe [43] and $Ni_{50}Al_{50}$ [29] (see [45, 48]).

All present calculations have been made using material parameters for $Cu_{50}Zr_{50}$ from table 2, where the relaxation time $\tau_\phi$, the diffusion factor $D_\phi^0$ and the energetic barrier $E_A$ are considered as free parameters at a fixed pseudo-glass transition temperature, $T_{AB}$. They can be obtained from molecular dynamics simulation (e.g. $\tau_\phi$) and from phase-field simulations (e.g. $D_\phi^0$ and $E_A$). The interface width $\eta_{int}$ has been taken from table 1 using KEA and double-well potential.

Figure 1 presents two bell-shaped curves given by solutions of (73)–(77). These solutions are plotted for the crystallization with the local non-equilibrium effect ($\tau_\phi \neq 0$, $V_\phi^B$ is finite) and without it ($\tau_\phi \to 0$, $V_\phi^B \to \infty$). With no local non-equilibrium effects ($\tau_\phi \to 0$), the predicted velocity well describes data of atomistic modeling only at small undercooling (see dashed curve obtained with the Set 1 from table 2 providing the better fit to data of simulations). If, however, the local non-equilibrium effect is included ($\tau_\phi \neq 0$), we recover perfectly the atomistic simulation data in the entire undercooling range and the growth rate (see solid curve obtained with Set 2 from table 2). The solidification kinetics of glass-forming alloys is well described by the theory which includes local non-equilibrium effects in the form of relaxation of the gradient flow in the phase-field. Therefore, good comparison with molecular dynamics data confirms our theoretical assumption using the phase-field models about the predominant influence of local non-equilibrium effects in crystal growth under large driving forces.

We finally note that the kinetic data of Tang and Harrowell obtained in atomistic simulations (see open squares in figure 1) are larger approximately for one order of magnitude

from those obtained experimentally on $Cu_{50}Zr_{50}$ samples for the whole undercooling balance (in which not only the kinetic undercooling $\Delta T_k$ but also contributions from the thermal transport and interface curvature are taken into account [48]). The kinetic data of Tang and Harrowell [29] also do not take into account a possible transformation of the cluster structure in $Cu_{50}Zr_{50}$ melt, which changes from a mixture of single icosahedral clusters to the mixture of interconnected clusters, long chains and even networks of the clusters as the undercooling increases [49]. This transformation may lead to the sharp drop off the interface velocity and even to the zero crystallization kinetics approximately one hundred Kelvin before the formation of the glassy phase in the $Cu_{50}Zr_{50}$ alloy [50]. Therefore, our present comparison with the data given by Tang and Harrowell [29] only demonstrates the ability to describe the bell-shaped kinetic curves, figure 1, characterizing the crystallization of glass-forming alloys.

## 7. Conclusions

The phase-field equations have been derived using an effective mobility approach and kinetic energy approach. These equations take into account relaxation of the phase-field variable $\phi$ and relaxation of the gradient flow $\partial\phi/\partial t$ that leads to the partial differential equations of the hyperbolic type. Using the double-well and double-obstacle potentials, the unified hodograph equation is found. Having the common form, this equation presents acceleration and velocity-dependent Gibbs–Thomson type of equation for the small, intermediate and large driving forces on the crystallization of pure substances or binary mixtures.

The kinetic equation for the slow and fast interface motion has been obtained from the unified hodograph equation for the steady-state crystal growth with constant velocity. A good comparison of the kinetic equation solution with molecular dynamics data on crystallization kinetics of the $Cu_{50}Zr_{50}$ alloy melt has been found. This quantitative comparison confirms the idea of the predominant influence of local non-equilibrium effects in fast crystallization under large driving forces.

## Acknowledgments

## ORCID iDs

A Salhoumi ● https://orcid.org/0000-0002-9288-1196
P K Galenko ● https://orcid.org/0000-0003-2941-7742

## References

[1] Levich V G 1962 *Physicochemical Hydrodynamics* (Englewood Cliffs, NJ: Prentice-Hall)

[2] Schneider F 1985 *Oscillations and Traveling Waves in Chemical Systems* ed R J Field and M Burger (New York: Wiley)

[3] Ward M J 2006 Asymptotic methods for reaction-diffusion systems: past and present *Bull. Math. Biol.* **68** 1151–67

[4] Mendez V, Fedotov S and Horsthemke W 2010 *Reaction-Transport Systems: Mesoscopic Foundations, Fronts, and Spatial Instabilities* (New York: Springer)

[5] Galenko P K, Sanches F I and Elder K R 2015 Traveling wave profiles for a crystaline front invading liquid states *Physica* D **308** 1–10

[6] Akamatsu S and Faivre G 2000 Traveling waves, two-phase fingers, and eutectic colonies in thin-sample directional solidification of a ternary eutectic alloy *Phys. Rev.* E **61** 3757

[7] Malfliet W and Hereman W 1996 The tanh method: exact solutions of nonlinear evolution and wave equations *Phys. Scr.* **54** 563–8

[8] Malfliet W 2004 The tanh method: a tool for solving certain classes of nonlinear evolution and wave equations *J. Comput. Appl. Math.* **164–5** 529–41

[9] Fan E 2002 Multiple travelling wave solutions of nonlinear evolution equations using a unified algebraic method *J. Phys. A: Math. Gen.* **35** 6853–72

[10] Wazwaz A M 2004 The tanh method for traveling wave solutions of nonlinear equations *Appl. Math. Comput.* **154** 713–23

[11] Grasselli M, Petzeltova H and Schimperna G 2006 Convergence to stationary solutions for a parabolic-hyperbolic phase-field system *Commun. Pure Appl. Anal.* **5** 827–38

[12] Taşcan F and Bekir A 2009 Travelling wave solutions of Cahn–Allen equation by using first integral method *Appl. Math. Comput.* **207** 279–82

[13] Nizovtseva I G, Galenko P K and Alexandrov D V 2016 The hyperbolic Allen–Cahn equation: exact solutions *J. Phys. A: Math. Theor.* **49** 435201

[14] Kobayashi R 1994 A numerical approach to three-dimensional dendritic solidification *Exper. Math.* **3** 59–81

[15] Wheeler A A, Boettinger W J and McFadden G B 1992 Phase-field model for isothermal phase transitions in binary alloys *Phys. Rev.* A **45** 7424–39

[16] Danilov D 2003 Planar solidification from undercooled melt: an approximation of a dilute binary alloy for a phase-field model *Interface and Transport Dynamics (Lecture Notes in Computational Science and Engineering* vol 32) ed H Emmerich *et al* (Berlin: Springer) p 150

[17] Montroll E W 1972 Nonlinear rate processes, especially those involving competitive processes *Statistical Mechanics: New Concepts, New Problems, New Applications* ed S A Rice *et al* (Chicago, IL: University of Chicago Press) p 69

[18] Harrowell P R and Oxtoby D W 1987 On the interaction between order and a moving interface: dynamical disordering and anisotropic growth rates *J. Chem. Phys.* **86** 2932–42

[19] Steinbach I 2009 Phase-field models in materials science *Modelling Simul. Mater. Sci. Eng.* **17** 073001

[20] Galenko P K, Abramova E V, Jou D, Danilov D A, Lebedev V G and Herlach D M 2011 Solute trapping in rapid solidification of a binary dilute system: a phase-field study *Phys. Rev.* E **84** 041143

[21] Zhang L, Danilova E V, Steinbach I, Medvedev D and Galenko P K 2013 Diffuse-interface modeling of solute trapping in rapid solidification: predictions of the hyperbolic phase-field model and parabolic model with finite interface dissipation *Acta Mater.* **61** 4155–68

[22] Galenko P K and Jou D 2019 Rapid solidification as non-ergodic phenomenon *Phys. Rep.* **818** 1–70

[23] Luzzi R, Vasconcellos A R, Casas-Vázquez J and Jou D 1988 On the selection of the state space in nonequilibrium thermodynamics *Physica* A **248** 111–37

[24] Jou D, Casas-Vázquez J and Lebon G 2010 *Extended Irreversible Thermodynamics* 4th edn (Berlin: Springer)

[25] Galenko P and Jou D 2005 Diffuse-interface model for rapid phase transformations in non-equilibrium systems *Phys. Rev.* E **71** 046125

[26] Galenko P and Jou D 2009 Kinetic contribution to the fast spinodal decomposition controlled by diffusion *Physica* A **388** 3113–23

[27] Wang H, Galenko P K, Zhang X, Kuang W, Liu F and Herlach D M 2015 Phase-field modeling of an abrupt disappearance of solute drag in rapid solidification *Acta Mater.* **90** 282–91

[28] Salhoumi A and Galenko P K 2016 Gibbs–Thomson condition for the rapidly moving interface in a binary system *Physica* A **447** 161–71

[29] Tang C and Harrowell P 2013 Anomalously slow crystal growth of the glass-forming alloy $Cu_{50}Zr_{50}$ *Nat. Mater.* **12** 507–11

[30] Moelans N 2011 A quantitative and thermodynamically consistent phase-field interpolation function for multi-phase systems *Acta Mater.* **59** 1077–86

[31] Sou S 1971 *Hydrodynamics of Multiphase Systems* (Moscow: Mir) p 536

[32] Drew D A 1983 Mathematical modeling of two-phase flow *Annu. Rev. Fluid Mech.* **15** 261–91

[33] Vorobiov I L 1980 Mathematical modeling of castings crystallization *Proc. Bauman-MVTU* **30** 31–41

[34] Zhuravlev V A and Kitaev E M 1974 *Thermophysics of Continuous Ingot Formation* (Moscow: Metallurgia)

[35] Beckermann C, Diepers H-J, Steinbach I, Karma A and Tong X 1999 Modeling melt convection in phase-field simulations of solidification *J. Comput. Phys.* **154** 468–96

[36] Hassanizadeh M and Gray W G 1979 General conservation equations for multi-phase systems: 1. Averaging procedure *Adv. Water Resour.* **2** 131–44

[37] Ni J and Beckermann C 1991 A volume-averaged two-phase model for transport phenomena during solidification *Metall. Trans.* B **22** 349–61

[38] Caginalp G 1989 Stefan and Hele–Shaw type models as asymptotic limits of the phase-field equation *Phys. Rev.* A **39** 5887–96

[39] Svoboda J, Turek I and Fischer F D 2005 Application of the thermodynamic extremal principle to modeling of thermodynamic processes in material sciences *Phil. Mag.* **85** 3699–707

[40] Fischer F D, Svoboda J and Petryk H 2014 Thermodynamic extremal principles for irreversible processes in materials science *Acta Mater.* **67** 1–20

[41] Wang H F, Liu F, Ehlen G J and Herlach D M 2013 Application of the maximal entropy production principle to rapid solidification: a multi-phase-field model *Acta Mater.* **61** 2617–27

[42] Salhoumi A and Galenko P K 2017 Analysis of interface kinetics: solutions of the Gibbs–Thomson-type equation and of the kinetic rate theory *IOP Conf. Ser.: Mater. Sci. Eng.* **192** 12014

[43] Ashkenazy Y and Averback R S 2007 Atomic mechanisms controlling crystallization behaviour in metals at deep undercoolings *Europhys. Lett.* **79** 26005

[44] Kerrache A, Horbach J and Binder K 2008 Molecular-dynamics computer simulation of crystal growth and melting in $Al_{50}Ni_{50}$ *Europhys. Lett.* **81** 58001

[45] Galenko P K and Ankudinov V 2019 Local non-equilibrium effect on the growth kinetics of crystals *Acta Mater.* **168** 203–9

[46] Galenko P K, Ankudinov V, Reuther K, Rettenmayr M, Salhoumi A and Kharanzhevskiy E V 2019 Thermodynamics of rapid solidification and crystal growth kinetics in glass-forming alloys *Phil. Trans. R. Soc.* A **377** 20180205

[47] Wang Q, Wang L M, Ma M Z, Binder S, Volkmann T, Herlach D M, Wang J S, Xue Q G, Tian Y J and Liu R P 2011 Diffusion-controlled crystal growth in deeply undercooled melt on approaching the glass transition *Phys. Rev.* B **83** 014202

[48] Galenko P K, Salhoumi A and Ankudinov V 2019 Kinetics of rapid crystal growth: phase field theory versus atomistic simulations *IOP Conf. Ser.: Mat. Sci. Eng.* **529** 012035

[49] Soklaski R, Nussinov Z, Markow Z, Kelton K F and Yang L 2013 Connectivity of icosahedral network and a dramatically growing static length scale in Cu–Zr binary metallic glasses *Phys. Rev.* B **87** 184203

[50] Galenko P K, Wonneberger R, Koch S, Ankudinov V, Kharanzhevskiy E V and Rettenmayr M 2020 Bell-shaped 'dendrite velocity-undercooling' relationship with an abrupt drop of solidification kinetics in glass forming Cu–Zr(–Ni) melts *J. Cryst. Growth* **532** 125411